Identification of Lipid Droplet Targeting Motifs and Mechanisms for Lipolytic Inhibitors G0S2 and HIG2

Latoya E. Campbell[1,3], Aaron M. Anderson[1,4], Yongbin Chen[1], Scott M. Johnson[1,5], Cailin E. McMahon[1], and Jun Liu[1,2,*]

From Department of Biochemistry and Molecular Biology[1], Mayo Clinic College of Medicine & Science, Rochester, Minnesota 55905, USA; Division of Endocrinology, Diabetes, Metabolism and Nutrition[2], Mayo Clinic in Rochester, Rochester, Minnesota 55905, USA; College of Health Solutions[3], Arizona State University, Tempe, Arizona 85281, USA; Department of Developmental Biology[4], Washington University School of Medicine in St. Louis, St. Louis, Missouri 63110, USA; Mayo Clinic Graduate School of Biomedical Sciences[5], Rochester, MN, 55905, USA[5].

[*]To whom correspondence should be addressed: Jun Liu, Guggenheim Building 14-11A, 222 3rd Avenue SW, Rochester, MN 55905. Phone: 507-284-8120; E-mail: liu.jun@mayo.edu

Keywords: lipid droplet, localization, lipolysis, lipase, inhibitor, motif, endoplasmic reticulum.

Summary statement

We identify structural determinants and mechanisms for LD targeting of G0S2 and HIG2, two known inhibitors of intracellular lipolysis.

ABSTRACT

G0S2 and HIG2 are two selective inhibitors of ATGL, the key enzyme for intracellular lipolysis. While G0S2 regulates triglyceride (TG) mobilization in adipocytes and hepatocytes, HIG2 functions to enhance intracellular TG accumulation under hypoxic conditions. A homologous hydrophobic domain (HD) is shared by G0S2 and HIG2 for binding to ATGL. However, the determinants of their lipid droplet (LD) localization are unknown. Here, we study how G0S2 and HIG2 are targeted to LDs, and identify both ATGL-independent and –dependent mechanisms.

Structural prediction and studies in cells reveal that ATGL-independent localization of G0S2 to both ER and LDs is mediated by a hairpin structure consisting of two hydrophobic sequences. Positively charged residues in the hinge region play a crucial role in sorting G0S2, which initially localizes at ER, to LDs. Interestingly, the role of these positive charges becomes dispensable when ATGL is co-expressed. In comparison, HIG2, which lacks a similar hairpin structure, is dependent on ATGL for its full LD targeting. Thus, our studies identify specific structural features and mechanisms for mediating accumulation of these two ATGL inhibitors on LDs.

INTRODUCTION

Lipid droplets (LDs) are composed of a neutral lipid core coated by a phospholipid monolayer, and are dynamic organelles critically involved in triglyceride (TG) storage and breakdown (Kory et al., 2016; Walther et al., 2017). In response to fasting or nutrient deprivation, TG stores in LDs undergo a hydrolytic process termed lipolysis to release fatty acids (FAs) (Grabner et al., 2021; Zechner et al., 2017). The highest activities of intracellular lipolysis are observed in adipose tissue, followed by oxidative tissues such as striated muscles and liver. The biochemical process is likewise conserved in adipocytes and non-adipocyte cells, where adipose tissue triglyceride lipase (ATGL) is the rate-limiting enzyme acting at the LD surface to catalyze hydrolysis of TG to one free FA and one diglyceride (DG) (Bezaire et al., 2009; Girousse and Langin, 2012; Jenkins et al., 2004; Villena et al., 2004; Zechner et al., 2009; Zechner et al., 2012; Zimmermann et al., 2004). Structurally, the N-terminal region of ATGL contains a predicted three-layer α/β-hydrolase fold and an overlapping patatin-like domain, which harbors an unconventional serine-aspartate catalytic dyad similar to the one found in cytosolic phospholipase A_2 ($cPLA_2$) (Dessen et al., 1999). The C-terminal region of ATGL, on the other hand, contains a hydrophobic lipid-binding domain (LBD) of 45 amino acids that are critical for LD targeting (Lu et al., 2010; Schweiger et al., 2008). Deletion of this LBD, as often observed in ATGL mutants associated with neutral lipid storage disease with myopathy (NLSDM), produces truncated proteins that lose LD-associated lipase activity *in vivo* (Fischer et al., 2007; Kobayashi et al., 2008; Schweiger et al., 2009).

Aside from its LD localization, the ability of ATGL to hydrolyze TG at the LD surface is tightly controlled by its interaction with other regulatory proteins (Cerk et al., 2018). While the lipolytic activity of ATGL is coactivated by comparative gene identification-58 (CGI-58) (Lass et al., 2006), ATGL-mediated lipolysis can be inhibited by G0/G1 switch gene 2 (G0S2) (Yang et al., 2010) and the recently identified hypoxia-inducible gene 2 (HIG2)/hypoxia-inducible lipid droplet-associated (HILPDA) (Padmanabha Das et al., 2018; Zhang et al., 2017b). G0S2 is a 103-amino acid protein primarily expressed in hepatocytes and adipocytes in response to elevation in intracellular FA levels. G0S2 is a basic protein that contains a central hydrophobic domain (HD). Through direct interaction with the patatin-like domain of ATGL, the sequence encompassing the G0S2 HD domain mediates the noncompetitive inhibition of ATGL with an IC_{50} in the nanomolar range (Cerk et al., 2014; Padmanabha Das et al., 2018). Functional studies using various mouse models have demonstrated that the interplay between ATGL and G0S2 is critical for balancing tissue-specific TG storage *vs.* mobilization as well as for partitioning of metabolic fuels between adipose tissue and liver (Choi et al., 2014; El-Assaad et al., 2015; Heckmann et al., 2014; Heier et al., 2015; Ma et al., 2014; Nielsen and Moller, 2014; Shin et al., 2014; Sugaya and Satoh, 2016; Wang et al., 2013; Zhang et al., 2017a; Zhang et al., 2014).

In comparison to G0S2, HIG2 is a 63-amino acid protein that contains a HD domain similar to that of G0S2 (Povero et al., 2020). Like G0S2, HIG2 inhibits ATGL through direct physical association (Padmanabha Das et al., 2018; Zhang et al., 2017b). In various types of cells, hypoxia upregulates HIG2 expression and promotes TG-LD accumulation through HIG2-mediated ATGL inhibition (van Dierendonck et al., 2020; van Dierendonck et al., 2022; VandeKopple et al., 2019; Zhang et al., 2017b). In hypoxic cancer cells, lipolytic inhibition is a defense mechanism against hypoxia-induced oxidative stress as it triggers downregulation of PPARα target genes for mitochondrial activity and FA β-oxidation, leading to decreased reactive oxygen species (ROS) generation and apoptotic cell death (Zhang et al., 2017b). Though it is a weaker ATGL inhibitor than G0S2 in *in vitro* biochemical assays (Padmanabha Das et al., 2018), HIG2's function appears to be ATGL-specific *in vivo* as co-deletion of ATGL was able to completely reverse the phenotypes caused by HIG2 deficiency in both cancer cells and macrophages (van Dierendonck et al., 2022; Zhang et al., 2017b).

On the cellular level, HIG2 and G0S2 both inhibit basal and CGI-58-activated ATGL at the LD surface (Lu et al., 2010; Padmanabha Das et al., 2018; Yang et al., 2010). While ATGL localization to LDs is mediated by the Arf1–coat protein complex I (COPI) machinery (Beller et al., 2008; Ellong et al., 2011; Soni et al., 2009; Suzuki et al., 2015), the mechanisms and structural basis for targeting G0S2 and HIG2 to LDs remain undefined. In this study, we show that while LD localization of HIG2 is fully dependent on ATGL, G0S2 can be targeted from ER to LDs via both ATGL-independent and –dependent mechanisms. Moreover, we use mutagenesis and cell imaging experiments to demonstrate that a hairpin loop formed by two helices at the N-terminal region of G0S2 is essential for anchoring the protein to ER prior to translocation to LDs. Furthermore, we found that basic residues within the hinge sequence of the hairpin play an important role in sorting of ER-localized G0S2 to LDs.

RESULTS

G0S2 localizes to LDs upon either LD induction or ATGL association

G0S2 plays an important role in regulating ATGL-mediated intracellular lipolysis in liver and adipose tissue (Zhang et al., 2017a). To determine whether the LD localization of G0S2 is dependent on its physical interaction with ATGL, we expressed mouse G0S2 in primary hepatocytes isolated from ATGL knockout mice via adenoviral infection. A FLAG epitope tag fused at its C-terminus of G0S2 (G0S2-FLAG) allowed examination of its localization using immunofluorescence staining. As shown in Figure 1A and 1B, G0S2 was mainly localized at honeycomb-like structures that resemble ER tubules and cisternae when cells were maintained in regular media without extra FA. However, after oleic acid was added to induce LD formation, G0S2 became highly enriched at the surface of LDs, which were stained with the neutral lipid dye Bodipy 493/503. Interestingly, coexpression of Myc-tagged ATGL resulted in the enrichment of FLAG-G0S2 with ATGL at the LD surface regardless of oleic acid treatment (Figure 1C and 1D). These results suggest that G0S2 is targeted to LDs via ATGL-independent and –dependent mechanisms, the former of which coincides with the induction of new LD formation.

G0S2 translocates from ER to LD after FA loading

G0S2 is known to localize at both ER and LDs (Yang et al., 2010; Zandbergen et al., 2005). To investigate the dynamic distribution of G0S2 between these two subcellular loci, we transiently transfected HeLa cells with mouse G0S2-FLAG and then examined its localization by immunofluorescence staining. Given their capacity to form and breakdown LDs, HeLa cells have been widely used as a cell biology model for studying LD association of ATGL and its regulatory proteins (Ellong et al., 2011; Keenan et al., 2021; Lu et al., 2010; Smirnova et al., 2006; Soni et al., 2009; Yang et al., 2010; Zhang et al., 2017b). To reveal the ER structure, cells were co-transfected with GFP-tagged Sec61, a general ER marker. To visualize intracellular LDs, cells were stained with LipidTOX dye following fixation. Initially, transfected cells were incubated in the presence of lipoprotein-deprived serum to reduce LDs (referred to as lipid starvation). In response to lipid starvation, G0S2 was found in small punctate structures apparently connected to the ER (at time 0 min, Figure 2) while mature LDs were not visible. After 5 min of oleic acid loading, G0S2 had already accumulated in rounded structures consistently connected to the ER. LipidTOX staining revealed these structures as newly formed LDs as they contained a core of neutral lipids. When starved cells were loaded with oleic acid for 15 min, some G0S2 coated LDs had enlarged and detached from ER. By 45-min time point post oleic acid loading, a majority of G0S2 protein was localized at the surface of LDs that were detached from ER. G0S2-coated LDs were almost completely separated from ER after 15 h of OA loading (Figure 2). These results suggest that lipid arrival promotes segregation of G0S2 within the ER into newly formed LDs.

A hydrophobic hairpin in G0S2 contains a positively charged ER-LD sorting signal

Many proteins appear to access the LD surface by one of two major pathways – from the ER or from the cytosol (Olarte et al., 2022). G0S2 appears to belong to the Class I LD proteins that have a dual localization in the ER and LDs. According to the AlphaFold structure prediction (Jumper et al., 2021; Varadi et al., 2022), the N-terminal portion of G0S2 consists of two α helices separated by a positively charged hinge sequence (Supplemental Figure 1). Together they form a V-shaped hairpin loop structure that may be capable of embedding in the phospholipid monolayer. To determine their individual involvement in ER and LD localization, we deleted each of the three sequences in the hairpin of mouse G0S2 as indicated in Figure 3A and co-

expressed the derived mutants in HeLa cells with GFP-Sec61. After oleic acid treatment, immunofluorescence staining revealed that the full-length, wild type protein is localized to the rim-like structures that resemble the surface of LDs and are separate from the ER (Supplementary Figure 2, Figure 3B and 3C). In comparison, deletion of any of the three sequences in the hairpin rendered the protein incapable of localizing to the LD surface rims (Supplementary Figure 2). A majority of G0S2Δ1-15, which lacks the first α helix, existed as punctae partially overlapping with the ER (Figure 3B and 3C). Deletion of the second α helix (Δ27-42/ΔHD) led to a tubule-like distribution that also only partially overlapped with ER. Strikingly, deletion of the hinge sequence (residues 16-26) resulted in a complete ER colocalization (Figure 3B and 3C). Together, these results indicate the importance of an intact hairpin structure in targeting G0S2 to ER as well as to LDs, and a critical role of the hinge sequence within the hairpin in mediating the exit of G0S2 from ER.

To further determine the role of the positive charges in the hinge sequence, we mutated three basic residues, individually or in combination, to the neutrally charged alanine. The FLAG-tagged mutant proteins were overexpressed in HeLa cells, which then were treated with oleic acid to promote LD formation. As shown in Figure 4A and 4B, both K25A single mutant and K22A/K25A double mutant retained the ability to traffick to LDs, whereas R20A/K22A/K25A triple mutant was disabled in LD localization. As a result, the triple mutant was completely restricted at the ER as revealed by its co-localization with the ER marker Sec61 (Figure 4C). These results suggest that the positive charges in the hinge sequence are a critical part of the LD targeting motif in G0S2 that sorts G0S2 from ER to LD.

ATGL-interaction motif within the G0S2 HD domain is not required for LD localization

The HD domain (residues 27-47; i.e. second putative α helix) in G0S2 is essential for both ATGL interaction and LD localization. To determine whether this ATGL-interacting domain is involved in LD localization, we coexpressed mouse ATGL tagged N-terminally with Myc (Myc-ATGL) with a series of deletion mutants of mouse G0S2 tagged C-terminally with FLAG, each lacking a 4-residue sequence in the HD domain (Figure 5A). The G0S2-ATGL interaction was then determined by co-immunoprecipitation analysis. As shown in Figure 5B, all G0S2-FLAG variants were expressed at comparable levels. When compared to the full-length protein, the

G0S2 mutant lacking the entire HD domain (G0S2Δ27-42) showed an almost complete loss of interaction with ATGL. Interestingly, deletion of each of the three 4-residue sequences in the C-terminal 12 residues of the HD, namely Δ31–34, Δ35–38 and Δ39-42, failed to significant affect the binding to ATGL. In comparison, the ATGL interaction with G0S2Δ27-30, the mutant that lacks first four-residue sequence YVLG, was largely disrupted (Figure 5B). This result is in agreement with our previous finding that the YVLG motif is critically needed for mediating inhibition of ATGL activity (Zhang et al., 2017b). To determine if loss of ATGL interaction was due to loss of G0S2' ability to localize to LD surface, we overexpressed wild type G0S2 or deletion mutants of G0S2 HD domain in ATGL$^{-/-}$ HeLa cells we generated previously (Varadi et al., 2022). While deletion of the entire HD domain abolished the G0S2's presence at the LD surface (Figure 3), lack of the ATGL-interacting YVLG motif in the HD domain did not affect the LD localization of G0S2Δ27-30 (Figure 5C). Neither did deletion of any other four-residue sequences in the HD. The results clearly demonstrate that though it requires the HD, the LD localization of G0S2 does not involve the ATGL-interaction motif.

ATGL binding promotes LD localization of R20A/K22A/K25A triple **mutant of G0S2**

Our results indicate that the positively charged hinge sequence facilitates the sorting of G0S2 from ER to LD. To determine whether the basic residues involved are also involved in mediating ATGL inhibition, we performed a TG hydrolase activity assay by using extracts of HeLa cells overexpressing ATGL as a lipase source. As shown in Figure 6A, addition of cell extracts containing wild type G0S2 or the R20A/K22A/K25A triple mutant both led to substantial inhibition of ATGL, indicating that the positive charges proximal to the N-terminal end of the ATGL-interacting HD domain are not required for the lipolytic inhibitory activity of G0S2. When expressed alone in HeLa cells, the ER-localized R20A/K22A/K25A mutant showed no noticeable presence at the LDs in response to oleic loading (Figure 6B). Interestingly, when coexpressed with ATGL, a significant amount of R20A/K22A/K25A mutant was detected along with ATGL at the LD surface.

A hydrophobic LBD (residues 259–337) in its C-terminal region is known to anchor ATGL to the surface of LDs. As described previously, deletion of this LD-anchoring LBD (as seen in ATGL/ΔLBD) prevented ATGL from localizing to LDs, a phenotype that was rescued when the

wild type G0S2 was coexpressed (Lu et al., 2010). Intriguingly, while individually they were both deficient in LD localization, ATGL/ΔLBD and G0S2/R20A/K22A/K25A mutants were able to traffick to LDs together when coexpressed in HeLa cells (Figure 6C). The result suggests that interaction with ATGL, but not the ability of ATGL to anchor to LDs, stimulates the translocation of G0S2/R20A/K22A/K25A mutant to LDs. Indeed, the LD recruitment by both WT and ΔLBD mutant of ATGL was abolished upon further deletion of the ATGL-binding motif in the triple mutant of G0S2 (R20A/K22A/K25A/Δ27-30) (Figure 6B and 6C).

ATGL regulates localization of HIG2 between ER and LDs.

HIG2 inhibits ATGL using a similar HD domain as G0S2. However, based on the prediction by AlphaFold (Supplemental Figure 3) (Jumper et al., 2021; Varadi et al., 2022), HIG2 lacks the first α helix and a positively charged hinge sequence that form the putative hairpin-like loop structure in G0S2. To further examine how HIG2 localization would be impacted by LD formation, we expressed mouse HIG2 tagged at the C-terminus with a FLAG epitope tag (HIG2-FLAG) in ATGL$^{-/-}$ HeLa cells with the ER marker GFP-Sec61. Under the lipid starvation conditions, HIG2 exhibited punctate localization at the ER (Figure 7A). Upon 15 min of oleic acid to induce LD formation, HIG2 was concentrated in the dot-like structures at the ER with some of those dots flanking the newly formed LDs. After an overnight oleic acid treatment, a majority of HIG2 protein was found to localize at the interface between enlarged LDs and ER instead of the LD surface rims as exhibited by G0S2. Interestingly, coexpression of ATGL was sufficient to promote complete LD localization of HIG2 (Figure 7B). As observed with the G0S2/R20A/K22A/K25A triple mutant, such an effect of ATGL coexpression did not require the LD-anchoring LBD of ATGL. These data suggest that the full LD localization of HIG2, which lacks a putative hairpin structure and a positive charged sequence proximal to its HD, is ATGL-dependent. Furthermore, addition of the G0S2 hinge sequence to the N-terminus of full-length HIG2 (G0S2/HIG2 fusion 1) yielded a hybrid protein that partially localizes to LDs attached to ER (Figure 7C). In comparison, addition of both the 1st helix and the hinge sequence of G0S2 was able to fully drive the G0S2/HIG2 hybrid protein to LDs that are detached from ER. The data are in support of the concept that a complete hairpin is required for sorting the protein from ER onto the LD surface.

DISCUSSION

Understanding mechanisms controlling FA and TG metabolism are essential for developing ways to counteract the negative effects of their dysregulation. ATGL, with its role as the rate-limiting enzyme catalyzing intracellular lipolysis and FA release from TG-LDs, is central to this understanding. G0S2 and HIG2 are two small protein inhibitors of ATGL, and their conserved HD domain mediates the inhibitory interaction with ATGL. At cellular level, how these inhibitory proteins make their ways onto LDs, where they meet with ATGL, is still under investigation. In this work, we identified unique targeting mechanisms for localizing these inhibitor proteins to LDs. We found that G0S2 contains a putative hairpin-like structure for initial insertion to the ER, followed by sorting from the bulk of ER to LDs. The latter process is mediated by the positively charged hinge sequence connecting the two α helices in the hairpin. This positively charged hinge sequence, however, is dispensable for LD localization when G0S2 binds to ATGL. In comparison, the predicted structure of HIG2 lacks the 1st α helix and the hinge sequence that form the hairpin in G0S2. The structural difference likely explains why HIG2 is incapable of trafficking to LDs on its own and instead, is dependent on ATGL for its full LD localization.

G0S2 appears to belong to a general class of proteins that are initially localized to ER and then migrates to the LD surface during LD formation. Ingelmo-Torres et al. were the first to identify a localization signal for sorting proteins with a hydrophobic domain within the ER into LDs (Ingelmo-Torres et al., 2009). The presence of a positively charged sequence is the main feature of this signal that correlates with the subsequent targeting from ER to LDs. A recent study by Olarte et al. further identified minimal motifs for ER to LD (ERTOLD) targeting as a hydrophobic hairpin-like structure containing two phospholipid embedded domains and a connecting hinge region with positively-charged residues (Olarte et al., 2020). We found that the N-terminal portion of G0S2 shares these structural features, and deletion of the entire positively charged hinge region in hairpin abolished the LD localization of G0S2. Instead, the mutant protein adopted an even distribution completely overlapping the ER network, and was excluded from the LD-forming sites. The same effect was recreated upon concurrent mutation of three basic residues in the hinge sequence to neutrally charged alanine, suggesting that the positive charges play an active role in driving the LD migration of G0S2. Since mutating individual basic

residues had little effect on LD targeting compared to mutating all three, the sum of positive charges in the hinge region seems to be more crucial for the preference of G0S2 localization at the LD surface. Despite the well-defined role of positively charged sequence in LD targeting, the underlying biophysical mechanisms remain to be determined. In the ER membrane, those charged residues are thought to be stabilized by interacting with the phosphate group of the luminal phospholipid leaflet (Olarte et al., 2020; Olarte et al., 2022). When embedded in the phospholipid monolayer of LD surface, these charged residues can be then stabilized by water in the LD core. Notably, the hydration properties of simulated LD systems recently demonstrated ~10 times more water in the LD core than previously reported (Kim and Swanson, 2020).

As also suggested by simulations, tryptophan and tyrosine residues can help ERTOLD proteins achieve a lower free energy state in the oil phase of the LD due to hydrogen bonding with the head groups of phospholipids, the glycerol moieties of TG or coordinating water molecules (Olarte et al., 2020; Olarte et al., 2022). However, this is unlikely the case for G0S2 as its LD targeting hairpin contains no tryptophan. Moreover, tyrosine-27 (Y^{27}) within the ATGL-interacting HD domain (i.e. the 2^{nd} α helix) is the lone tyrosine in the G0S2 hairpin. As mapped by the deletion mutagenesis, ATGL inhibition requires the Y^{27}VLG motif, the first four residues of the HD. Consistently, loss of this conserved sequence motif also abolished the ATGL interaction and inhibitory activity of HIG2 (Zhang et al., 2017b). A most recent study further showed that the single Y^{27}G mutation in G0S2 resulted in complete loss of ATGL inhibition (Riegler-Berket et al., 2022). Despite its importance of this conserved tyrosine residue in regulating ATGL, however, Y^{27} does not seem to be required for LD targeting since deletion of the entire YVLG motif elicited no effect on the ATGL-independent LD localization. Furthermore, G0S2 does not contain a central proline in its hairpin hinge region as commonly found in other ERTOLD proteins (Olarte et al., 2022). Taken together, our observations suggest that the hairpin conformation of G0S2 may differ considerably from the one contained in other ERTOLD proteins, and additional mechanisms may contribute to its accumulation at the LD surface.

Our data indicate that ATGL binding enables a second mechanism for targeting G0S2 to LD. The fact that ATGL was able to recruit G0S2/R20A/K22A/K25A triple mutant to LDs suggests

that such a mechanism does not involve the positively charged ERTOLD sorting signal. However, such recruitment seems to require a direct interaction as deletion of the ATGL-interacting motif in the G0S2 triple mutant abolished its ATGL-mediated LD localization. To this end, we propose two potential scenarios for the interplay between G0S2 LD localization and ATGL interaction. One is for G0S2 and ATGL to traffick to LDs separately and form inhibitory complex after their arrival at the LD surface. Previous studies have shown that ATGL may partially exist in the cytosol (Villena et al., 2004; Zimmermann et al., 2004), but most ATGL is likely to exist in a membrane-bound form (Soni et al., 2009). Transport of ATGL to LDs requires both the Arf1/COPI machinery (Beller et al., 2008; Ellong et al., 2011; Soni et al., 2009; Suzuki et al., 2015) and association of its C-terminal LBD with LD phospholipid monolayer (Lu et al., 2010; Schweiger et al., 2008). Thus, while G0S2 follows the ERTOLD pathway via its hairpin-like structure, ATGL translocates to LDs through vesicular trafficking and via its LBD. Alternatively, the second scenario is for ATGL to bind to G0S2 at the ER and the two proteins subsequently migrate to LDs as a complex. In this case, ATGL binding to the G0S2 HD domain may trigger conformational change in the G0S2 hairpin, resulting in LD relocalization independently of the positively charged hinge sequence. Of note, we showed that the R20A/K22A/K25A triple mutant still retained the full capacity to inhibit ATGL, suggesting that these charged residues proximal to the HD domain are not essential for ATGL interaction. A somewhat surprising finding is that the LD translocation is not mediated by the LD-localization of ATGL, since the ATGL mutant lacking the LBD was still able to drive G0S2/R20A/K22A/K25A triple mutant to the LD surface. Interestingly, a previous study demonstrated that C-terminally truncated ATGL mutants, which lack the LBD, translocate to the LD upon coexpression with G0S2 (Schweiger et al., 2012).

Our data are in support of a similar ATGL-dependent mechanism for targeting HIG2 to LDs. Compared with G0S2, HIG2 is a shorter peptide with a lower content of basic residues. Maier et. al. showed that endogenous HIG2 is present at points of contact between ER and LDs and that knockout of the HIG2 gene prevents hypoxia-induced LD formation in macrophages (Maier et al., 2017). In agreement with this previous observation, our data showed that in ATGL knockout cells, HIG2 is only partially localized to ER during lipid starvation and mostly to the LD-ER interface upon LD formation. This is consistent with its lack of the first α helix and a charged

hinge sequence that form the predicted LD-targeting hairpin in G0S2. As a result, the full LD localization of HIG2 is dependent on ATGL, as evidenced by the fact that HIG2 only relocalizes to LDs upon ATGL coexpression. Similarly to that of G0S2/R20A/K22A/K25A triple mutant, such a LD relocalization of HIG2 does not seem to require the C-terminal LBD of ATGL. Mechanistically, how such a mutual LD recruitment occurs remains unclear. Given that HIG2 and G0S2 interact with the N-terminal patatin-like domain of ATGL, it is reasonable to assume that ATGL undergoes a so-called "folding-upon-binding" process upon interaction with these inhibitory proteins, which enables anchoring of ATGL to the phospholipid surface of the LDs without involving its C-terminal LBD. If so, it would be tempting to determine whether binding to the inhibitor proteins would induce dissociation of ATGL's LBD from the LD phospholipids. If so, whether such dissociation would prevent the physical contact of ATGL with the inner TG core of LDs, thereby impeding the hydrolytic action of ATGL.

MATERIALS AND METHODS

PCR cloning of cDNA and site-directed mutagenesis

The complete open reading frames of mouse ATGL, G0S2 and HIG2 were cloned into pRK vector with a FLAG or Myc epitope tag as previously reported (Yang et al., 2010; Zhang et al., 2017b). Deletion and point mutations were generated by using the QuickChange Site-Directed Mutagenesis Kit (Agilent Technologies) according to the manufacturer's guidelines. To generate G0S2/HIG2 hybrid expression constructs, we designed duplex oligonucleotides flanked by BamHI sites and encoding either the G0S2 hinge sequence alone or the 1st helix and the hinge sequence of G0S2. Upon BamHI digestion, these oligos were ligated into the BamHI site at the start of HIG2 cDNA sequence in the HIG2-FLAG vector. The correct insert orientation was verified by DNA sequencing and subsequent protein expression in transfected HeLa cells.

Adenoviral infection of mouse primary hepatocytes

Recombinant adenovirus encoding N-terminally Myc tagged ATGL and C-terminally FLAG tagged G0S2 under the control of a cytomegalovirus promoter were custom generated by Vector Biolabs. A cytomegalovirus-null virus [null adenovirus (Ad-Null)] was also obtained for use in control experiments. Primary mouse hepatocytes were isolated from male whole-body ATGL

knockout mice (C57BL/6 background) as described previously (Zhang et al., 2019) and in accordance with an approved protocol by the Institutional Animal Care and Use Committee at Mayo Clinic. Following isolation, primary hepatocytes were seeded into 6-well plates in the DMEM medium with low glucose and 1% fetal bovine serum at 37°C under 5% CO_2. Three hours later, cells were infected with 2×10^7 pfu per well of adenovirus for 40 h in the presence of 2.5 μg/ml of polybrene.

Transient transfection and protein analysis

Wild type or $ATGL^{-/-}$ HeLa cells as generate previously (Zhang et al., 2017b) were cultured in high glucose DMEM (Invitrogen) containing 10% FBS (Invitrogen) supplemented with 100 U ml−1 penicillin/streptomycin (Invitrogen). Cells at 70-80% confluence were transfected with plasmids expressing Myc-ATGL, G0S2-FLAG and/or HIG2-FLAG fusion proteins using Lipofectamine 2000. After overnight incubation with transfect mixtures, cells were lysed accordingly for downstream biochemical analyses. For immunoblotting, preparation of tissue and cell lysates and subsequent immunoblotting analysis were performed as described previously (Zhang et al., 2014). Briefly, following SDS-PAGE and transfer to nitrocellulose membranes, individual proteins were blotted with primary antibodies at appropriate dilutions. After an overnight incubation, peroxide-conjugated secondary antibodies were incubated with the membrane at a dilution of 1:5000. The signals were then visualized by chemiluminescence (Supersignal ECL, Pierce). For immunoprecipitation, cells were lysed in cell lysis buffer containing 50 mM Tris-HCl, pH 7.4, 150 mM NaCl, 1% Triton X-100, 1 mM DTT, and protease tablet inhibitors (1 mini tablet per 10 ml of buffer). Anti-Flag M2-conjugated gel was incubated with the lysates for 3 hrs at 4 °C. The beads were then washed four times with lysis buffer, and the bound proteins were eluted in SDS sample loading buffer and analyzed by immunoblotting.

Immunofluorescence and confocal microscopy

Cells were incubated with 400 μM oleic acid/0.2% BSA overnight to promote LD formation as described previously (Brasaemle and Wolins, 2006). Following the fixation with 4% paraformaldehyde in PBS for 15 min, cells were permeabilized by 0.25% triton X-100 for 5 min, quenched with 100 mM glycine in PBS for 20 min, and then blocked with 2% BSA in PBS for 1 hr. The cells were then exposed to primary antibody for 2 hr at room temperature. Following

three washes with PBS, the cells were treated for 1 hr with Alexa Fluor secondary antibodies. To visualize lipid droplets, 1 μg/ml of Bodipy 493/503 was added during the incubation with secondary antibodies. Alternatively, the cells were incubated in Deep Red LipidTOX dye at 1:2,000 dilution in PBS for 15 minutes after the secondary antibodies. Samples were mounted on glass slides with Vector Shield mounting medium and examined under a Zeiss LSM 980 inverted confocal microscope with Airyscan. Acquired images were processed and quantified manually with Zen Blue and ImageJ FIJI software.

Quantitative colocalization analysis

Colocalization analysis was performed using JACoP plugin embedded in ImageJ. LD colocalization of immunofluorescently stained proteins was determined quantitatively as described recently (Olarte et al., 2020). First, the LD-occupied region in each cell was identified based on Bodipy 493/503 staining. Specifically, an automatic threshold was applied to the raw images of BODIPY 493/503 channel. For each of the quantified cells, a mask was created via the Bodipy 493/503 channel that focuses on the LD-occupied region. The mean intensity of a given protein signal on LDs was divided by the mean intensity of the protein signal in the whole cell excluding LD-occupied region. Thus, the "LD enrichment factor" of individual proteins represents the ratio of mean pixel intensity and area of a protein signal (red) in the LD-occupied region relative to those in the whole cell excluding LDs.

For quantitative ER colocalization analysis, the co-localization threshold plugin was used to calculate the Pearson coefficient of co-localization with the ER marker GFP-Sec61. Each image was analyzed by creating a mask via the GFP-Sec61 channel that focuses on the region of interest (ROI) to the ER structures. The estimation of Pearson's correlation coefficient is applied for matching the fluorescence pixel intensities from a protein channel (red) to the ROI in order to describe the degree of overlap between a protein and ER, taking into account the environment of each pixel. A value of 1.0 is the result of complete co-localization between two channels. The Pearson coefficient was calculated for twenty cell images per condition. Bars represent the mean ± SD from each image.

In vitro transcription/translation expression

In vitro transcription/translation was carried out by using TNT SP6 High-Yield Protein Expression System (Promega) according to the manufacturer's instructions. Specifically, reactions consisting of 30 µL TNT SP6 High-Yield Wheat Germ Master Mix and 5 µg vector DNA, made up to 50 µL with molecular biology grade water were incubated for 120 min at 25°C. Then the reaction mixture was used for TG lipase activity or immunoblotting analysis.

Determination of TG hydrolase activity

A total of 35 µl of *in vitro* transcription/translation reaction mixture was prediluted with 65 µl of cell extraction buffer (0.25 M sucrose, 1 mM EDTA, 1 mM DTT). The TG hydrolase activity against ^{3}H-labeled triolein was measured as described previously (Zhang et al., 2013) by mixing 0.1 ml of diluted reaction mixture with 0.1 ml of substrate solution. Reactions were terminated by adding 3.25 ml of methanol/chloroform/heptane (10:9:7) and 1.0 mL of 0.1 M potassium carbonate, 0.1 M boric acid (pH 10.5). Following centrifugation at 800 × g for 15 min, radiolabeled FAs in 1 ml of upper phase were measured by liquid scintillation counting.

Statistical analysis

When evaluating the statistical difference between the mean values of two datasets, we used unpaired two-tailed Student's t test with Welch's correction. If the two datasets did not follow a normal distribution, we used the Mann–Whitney U test. One-sample t test was used in the case of normalized data. No statistical method was used to predetermine sample size.

ACKNOWLEDGEMENTS

We would like to thank Dr. Xiaodong Zhang, Alicia Saarinen and Joseph Webb for their excellent technical support. We are grateful that Dr. Rudolf Zechner kindly shared the ATGL knockout mice, from which primary hepatocytes were derived.

COMPETING INTERESTS

No competing interests declared.

FUNDING

This project was supported by research grants from the National Institutes of Health (DK089178 and DK109096) to J.L. as well as pre-doctoral funding to L.E.C. from the Initiative for Maximizing Student Development (IMSD) Program at Arizona State University.

REFERENCES

Beller, M., Sztalryd, C., Southall, N., Bell, M., Jackle, H., Auld, D. S. and Oliver, B. (2008). COPI complex is a regulator of lipid homeostasis. *PLoS Biol* **6**, e292.

Bezaire, V., Mairal, A., Ribet, C., Lefort, C., Girousse, A., Jocken, J., Laurencikiene, J., Anesia, R., Rodriguez, A. M., Ryden, M. et al. (2009). Contribution of adipose triglyceride lipase and hormone-sensitive lipase to lipolysis in hMADS adipocytes. *J Biol Chem* **284**, 18282-91.

Brasaemle, D. L. and Wolins, N. E. (2006). Isolation of lipid droplets from cells by density gradient centrifugation. *Curr Protoc Cell Biol* **Chapter 3**, Unit 3 15.

Cerk, I. K., Salzburger, B., Boeszoermenyi, A., Heier, C., Pillip, C., Romauch, M., Schweiger, M., Cornaciu, I., Lass, A., Zimmermann, R. et al. (2014). A Peptide Derived from G0/G1 Switch Gene 2 Acts as Non-competitive Inhibitor of Adipose Triglyceride Lipase. *The Journal of biological chemistry*.

Cerk, I. K., Wechselberger, L. and Oberer, M. (2018). Adipose Triglyceride Lipase Regulation: An Overview. *Curr Protein Pept Sci* **19**, 221-233.

Choi, H., Lee, H., Kim, T. H., Kim, H. J., Lee, Y. J., Lee, S. J., Yu, J. H., Kim, D., Kim, K. S., Park, S. W. et al. (2014). G0/G1 switch gene 2 has a critical role in adipocyte differentiation. *Cell death and differentiation* **21**, 1071-80.

Dessen, A., Tang, J., Schmidt, H., Stahl, M., Clark, J. D., Seehra, J. and Somers, W. S. (1999). Crystal structure of human cytosolic phospholipase A2 reveals a novel topology and catalytic mechanism. *Cell* **97**, 349-60.

El-Assaad, W., El-Kouhen, K., Mohammad, A. H., Yang, J., Morita, M., Gamache, I., Mamer, O., Avizonis, D., Hermance, N., Kersten, S. et al. (2015). Deletion of the gene encoding G0/G 1 switch protein 2 (G0s2) alleviates high-fat-diet-induced weight gain and insulin resistance, and promotes browning of white adipose tissue in mice. *Diabetologia* **58**, 149-57.

Ellong, E. N., Soni, K. G., Bui, Q. T., Sougrat, R., Golinelli-Cohen, M. P. and Jackson, C. L. (2011). Interaction between the triglyceride lipase ATGL and the Arf1 activator GBF1. *PLoS One* **6**, e21889.

Fischer, J., Lefevre, C., Morava, E., Mussini, J. M., Laforet, P., Negre-Salvayre, A., Lathrop, M. and Salvayre, R. (2007). The gene encoding adipose triglyceride lipase (PNPLA2) is mutated in neutral lipid storage disease with myopathy. *Nat Genet* **39**, 28-30.

Girousse, A. and Langin, D. (2012). Adipocyte lipases and lipid droplet-associated proteins: insight from transgenic mouse models. *International journal of obesity* **36**, 581-94.

Grabner, G. F., Xie, H., Schweiger, M. and Zechner, R. (2021). Lipolysis: cellular mechanisms for lipid mobilization from fat stores. *Nat Metab* **3**, 1445-1465.

Heckmann, B. L., Zhang, X., Xie, X., Saarinen, A., Lu, X., Yang, X. and Liu, J. (2014). Defective adipose lipolysis and altered global energy metabolism in mice with adipose overexpression of the lipolytic inhibitor G0/G1 switch gene 2 (G0S2). *The Journal of biological chemistry* **289**, 1905-16.

Heier, C., Radner, F. P., Moustafa, T., Schreiber, R., Grond, S., Eichmann, T. O., Schweiger, M., Schmidt, A., Cerk, I. K., Oberer, M. et al. (2015). G0/G1 Switch Gene 2 Regulates Cardiac Lipolysis. *The Journal of biological chemistry* **290**, 26141-50.

Ingelmo-Torres, M., Gonzalez-Moreno, E., Kassan, A., Hanzal-Bayer, M., Tebar, F., Herms, A., Grewal, T., Hancock, J. F., Enrich, C., Bosch, M. et al. (2009). Hydrophobic and basic domains target proteins to lipid droplets. *Traffic* **10**, 1785-801.

Jenkins, C. M., Mancuso, D. J., Yan, W., Sims, H. F., Gibson, B. and Gross, R. W. (2004). Identification, cloning, expression, and purification of three novel human calcium-independent phospholipase A2 family members possessing triacylglycerol lipase and acylglycerol transacylase activities. *J Biol Chem* **279**, 48968-75.

Jumper, J., Evans, R., Pritzel, A., Green, T., Figurnov, M., Ronneberger, O., Tunyasuvunakool, K., Bates, R., Zidek, A., Potapenko, A. et al. (2021). Highly accurate protein structure prediction with AlphaFold. *Nature* **596**, 583-589.

Keenan, S. N., De Nardo, W., Lou, J., Schittenhelm, R. B., Montgomery, M. K., Granneman, J. G., Hinde, E. and Watt, M. J. (2021). Perilipin 5 S155 phosphorylation by PKA is required for the control of hepatic lipid metabolism and glycemic control. *J Lipid Res* **62**, 100016.

Kim, S. and Swanson, J. M. J. (2020). The Surface and Hydration Properties of Lipid Droplets. *Biophys J* **119**, 1958-1969.

Kobayashi, K., Inoguchi, T., Maeda, Y., Nakashima, N., Kuwano, A., Eto, E., Ueno, N., Sasaki, S., Sawada, F., Fujii, M. et al. (2008). The lack of the C-terminal domain of adipose triglyceride lipase causes neutral lipid storage disease through impaired interactions with lipid droplets. *J Clin Endocrinol Metab* **93**, 2877-84.

Kory, N., Farese, R. V., Jr. and Walther, T. C. (2016). Targeting Fat: Mechanisms of Protein Localization to Lipid Droplets. *Trends in cell biology* **26**, 535-46.

Lass, A., Zimmermann, R., Haemmerle, G., Riederer, M., Schoiswohl, G., Schweiger, M., Kienesberger, P., Strauss, J. G., Gorkiewicz, G. and Zechner, R. (2006). Adipose triglyceride lipase-mediated lipolysis of cellular fat stores is activated by CGI-58 and defective in Chanarin-Dorfman Syndrome. *Cell Metab* **3**, 309-19.

Lu, X., Yang, X. and Liu, J. (2010). Differential control of ATGL-mediated lipid droplet degradation by CGI-58 and G0S2. *Cell Cycle* **9**, 2719-25.

Ma, T., Lopez-Aguiar, A. G., Li, A., Lu, Y., Sekula, D., Nattie, E. E., Freemantle, S. and Dmitrovsky, E. (2014). Mice lacking G0S2 are lean and cold-tolerant. *Cancer biology & therapy* **15**.

Maier, A., Wu, H., Cordasic, N., Oefner, P., Dietel, B., Thiele, C., Weidemann, A., Eckardt, K. U. and Warnecke, C. (2017). Hypoxia-inducible protein 2 Hig2/Hilpda mediates neutral lipid accumulation in macrophages and contributes to atherosclerosis in apolipoprotein E-deficient mice. *FASEB J* **31**, 4971-4984.

Nielsen, T. S. and Moller, N. (2014). Adipose triglyceride lipase and G0/G1 switch gene 2: approaching proof of concept. *Diabetes* **63**, 847-9.

Olarte, M. J., Kim, S., Sharp, M. E., Swanson, J. M. J., Farese, R. V., Jr. and Walther, T. C. (2020). Determinants of Endoplasmic Reticulum-to-Lipid Droplet Protein Targeting. *Dev Cell* **54**, 471-487 e7.

Olarte, M. J., Swanson, J. M. J., Walther, T. C. and Farese, R. V., Jr. (2022). The CYTOLD and ERTOLD pathways for lipid droplet-protein targeting. *Trends Biochem Sci* **47**, 39-51.

Padmanabha Das, K. M., Wechselberger, L., Liziczai, M., De la Rosa Rodriguez, M., Grabner, G. F., Heier, C., Viertlmayr, R., Radler, C., Lichtenegger, J., Zimmermann, R. et al. (2018). Hypoxia-inducible lipid droplet-associated protein inhibits adipose triglyceride lipase. *J Lipid Res* **59**, 531-541.

Povero, D., Johnson, S. M. and Liu, J. (2020). Hypoxia, hypoxia-inducible gene 2 (HIG2)/HILPDA, and intracellular lipolysis in cancer. *Cancer Lett* **493**, 71-79.

Riegler-Berket, L., Wechselberger, L., Cerk, I. K., Padmanabha Das, K. M., Viertlmayr, R., Kulminskaya, N., Rodriguez Gamez, C. F., Schweiger, M., Zechner, R., Zimmermann, R. et al. (2022). Residues of the minimal sequence of G0S2 collectively contribute to ATGL inhibition while C-and N-terminal extensions promote binding to ATGL. *Biochim Biophys Acta Mol Cell Biol Lipids* **1867**, 159105.

Schweiger, M., Lass, A., Zimmermann, R., Eichmann, T. O. and Zechner, R. (2009). Neutral lipid storage disease: genetic disorders caused by mutations in adipose triglyceride lipase/PNPLA2 or CGI-58/ABHD5. *Am J Physiol Endocrinol Metab* **297**, E289-96.

Schweiger, M., Paar, M., Eder, C., Brandis, J., Moser, E., Gorkiewicz, G., Grond, S., Radner, F. P., Cerk, I., Cornaciu, I. et al. (2012). G0/G1 switch gene-2 regulates human adipocyte lipolysis by affecting activity and localization of adipose triglyceride lipase. *J Lipid Res* **53**, 2307-17.

Schweiger, M., Schoiswohl, G., Lass, A., Radner, F. P., Haemmerle, G., Malli, R., Graier, W., Cornaciu, I., Oberer, M., Salvayre, R. et al. (2008). The C-terminal region of human adipose triglyceride lipase affects enzyme activity and lipid droplet binding. *J Biol Chem* **283**, 17211-20.

Shin, S., Choi, Y. M., Han, J. Y. and Lee, K. (2014). Inhibition of lipolysis in the novel transgenic quail model overexpressing G0/G1 switch gene 2 in the adipose tissue during feed restriction. *PLoS One* **9**, e100905.

Smirnova, E., Goldberg, E. B., Makarova, K. S., Lin, L., Brown, W. J. and Jackson, C. L. (2006). ATGL has a key role in lipid droplet/adiposome degradation in mammalian cells. *EMBO Rep* **7**, 106-13.

Soni, K. G., Mardones, G. A., Sougrat, R., Smirnova, E., Jackson, C. L. and Bonifacino, J. S. (2009). Coatomer-dependent protein delivery to lipid droplets. *J Cell Sci* **122**, 1834-41.

Sugaya, Y. and Satoh, H. (2016). Liver-specific G0 /G1 switch gene 2 (G0s2) expression promotes hepatic insulin resistance by exacerbating hepatic steatosis in male Wistar rats. *Journal of diabetes*.

Suzuki, M., Murakami, T., Cheng, J., Kano, H., Fukata, M. and Fujimoto, T. (2015). ELMOD2 is anchored to lipid droplets by palmitoylation and regulates adipocyte triglyceride lipase recruitment. *Mol Biol Cell* **26**, 2333-42.

van Dierendonck, X., de la Rosa Rodriguez, M. A., Georgiadi, A., Mattijssen, F., Dijk, W., van Weeghel, M., Singh, R., Borst, J. W., Stienstra, R. and Kersten, S. (2020). HILPDA Uncouples Lipid Droplet Accumulation in Adipose Tissue Macrophages from Inflammation and Metabolic Dysregulation. *Cell Rep* **30**, 1811-1822 e6.

van Dierendonck, X., Vrieling, F., Smeehuijzen, L., Deng, L., Boogaard, J. P., Croes, C. A., Temmerman, L., Wetzels, S., Biessen, E., Kersten, S. et al. (2022). Triglyceride breakdown from lipid droplets regulates the inflammatory response in macrophages. *Proc Natl Acad Sci U S A* **119**, e2114739119.

VandeKopple, M. J., Wu, J., Auer, E. N., Giaccia, A. J., Denko, N. C. and Papandreou, I. (2019). HILPDA Regulates Lipid Metabolism, Lipid Droplet Abundance, and Response to Microenvironmental Stress in Solid Tumors. *Mol Cancer Res* **17**, 2089-2101.

Varadi, M., Anyango, S., Deshpande, M., Nair, S., Natassia, C., Yordanova, G., Yuan, D., Stroe, O., Wood, G., Laydon, A. et al. (2022). AlphaFold Protein Structure Database: massively expanding the structural coverage of protein-sequence space with high-accuracy models. *Nucleic Acids Res* **50**, D439-D444.

Villena, J. A., Roy, S., Sarkadi-Nagy, E., Kim, K. H. and Sul, H. S. (2004). Desnutrin, an adipocyte gene encoding a novel patatin domain-containing protein, is induced by fasting and glucocorticoids: ectopic expression of desnutrin increases triglyceride hydrolysis. *J Biol Chem* **279**, 47066-75.

Walther, T. C., Chung, J. and Farese, R. V., Jr. (2017). Lipid Droplet Biogenesis. *Annu Rev Cell Dev Biol* **33**, 491-510.

Wang, Y., Zhang, Y., Qian, H., Lu, J., Zhang, Z., Min, X., Lang, M., Yang, H., Wang, N. and Zhang, P. (2013). The g0/g1 switch gene 2 is an important regulator of hepatic triglyceride metabolism. *PLoS One* **8**, e72315.

Yang, X., Lu, X., Lombes, M., Rha, G. B., Chi, Y. I., Guerin, T. M., Smart, E. J. and Liu, J. (2010). The G(0)/G(1) switch gene 2 regulates adipose lipolysis through association with adipose triglyceride lipase. *Cell Metab* **11**, 194-205.

Zandbergen, F., Mandard, S., Escher, P., Tan, N. S., Patsouris, D., Jatkoe, T., Rojas-Caro, S., Madore, S., Wahli, W., Tafuri, S. et al. (2005). The G0/G1 switch gene 2 is a novel PPAR target gene. *Biochem J* **392**, 313-24.

Zechner, R., Kienesberger, P. C., Haemmerle, G., Zimmermann, R. and Lass, A. (2009). Adipose triglyceride lipase and the lipolytic catabolism of cellular fat stores. *J Lipid Res* **50**, 3-21.

Zechner, R., Madeo, F. and Kratky, D. (2017). Cytosolic lipolysis and lipophagy: two sides of the same coin. *Nat Rev Mol Cell Biol* **18**, 671-684.

Zechner, R., Zimmermann, R., Eichmann, T. O., Kohlwein, S. D., Haemmerle, G., Lass, A. and Madeo, F. (2012). FAT SIGNALS--lipases and lipolysis in lipid metabolism and signaling. *Cell metabolism* **15**, 279-91.

Zhang, X., Heckmann, B. L., Campbell, L. E. and Liu, J. (2017a). G0S2: A small giant controller of lipolysis and adipose-liver fatty acid flux. *Biochim Biophys Acta* **1862**, 1146-1154.

Zhang, X., Heckmann, B. L. and Liu, J. (2013). Studying lipolysis in adipocytes by combining siRNA knockdown and adenovirus-mediated overexpression approaches. *Methods in cell biology* **116**, 83-105.

Zhang, X., Saarinen, A. M., Hitosugi, T., Wang, Z., Wang, L., Ho, T. H. and Liu, J. (2017b). Inhibition of intracellular lipolysis promotes human cancer cell adaptation to hypoxia. *Elife* **6**.

Zhang, X., Xie, X., Heckmann, B. L., Saarinen, A. M., Czyzyk, T. A. and Liu, J. (2014). Targeted disruption of g0/g1 switch gene 2 enhances adipose lipolysis, alters hepatic energy balance, and alleviates high-fat diet-induced liver steatosis. *Diabetes* **63**, 934-46.

Zhang, X., Xie, X., Heckmann, B. L., Saarinen, A. M., Gu, H., Zechner, R. and Liu, J. (2019). Identification of an intrinsic lysophosphatidic acid acyltransferase activity in the lipolytic inhibitor G0/G1 switch gene 2 (G0S2). *FASEB J* **33**, 6655-6666.

Zimmermann, R., Strauss, J. G., Haemmerle, G., Schoiswohl, G., Birner-Gruenberger, R., Riederer, M., Lass, A., Neuberger, G., Eisenhaber, F., Hermetter, A. et al. (2004). Fat mobilization in adipose tissue is promoted by adipose triglyceride lipase. *Science* **306**, 1383-6.

Figures

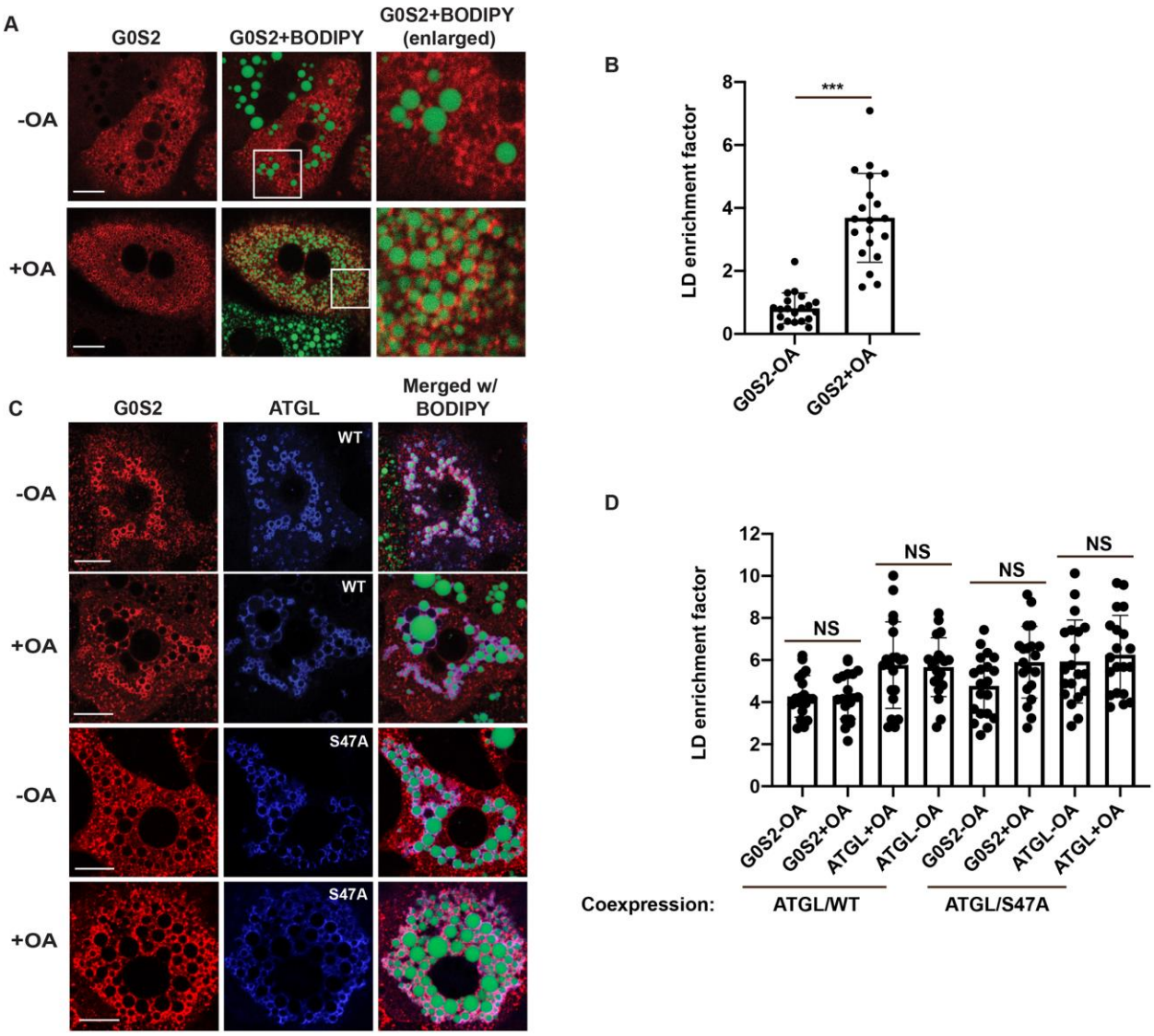

Fig. 1. Localization of G0S2 in mouse primary hepatocytes.

Lipid starved primary ATGL$^{-/-}$ hepatocytes expressing either G0S2-FLAG alone (A) or with Myc-ATGL (WT or S47A mutant) (C) were treated with or without OA overnight, and then imaged by immunofluorescence confocal microscopy. LDs were stained with BODIPY. Scale bar: 20 µm. The white box indicates the enlarged areas. Mean value + SD (n = 20) of the protein signal in (A) and (C) on LDs are shown in (B) and (D), respectively. ***p < 0.001; NS: no significance.

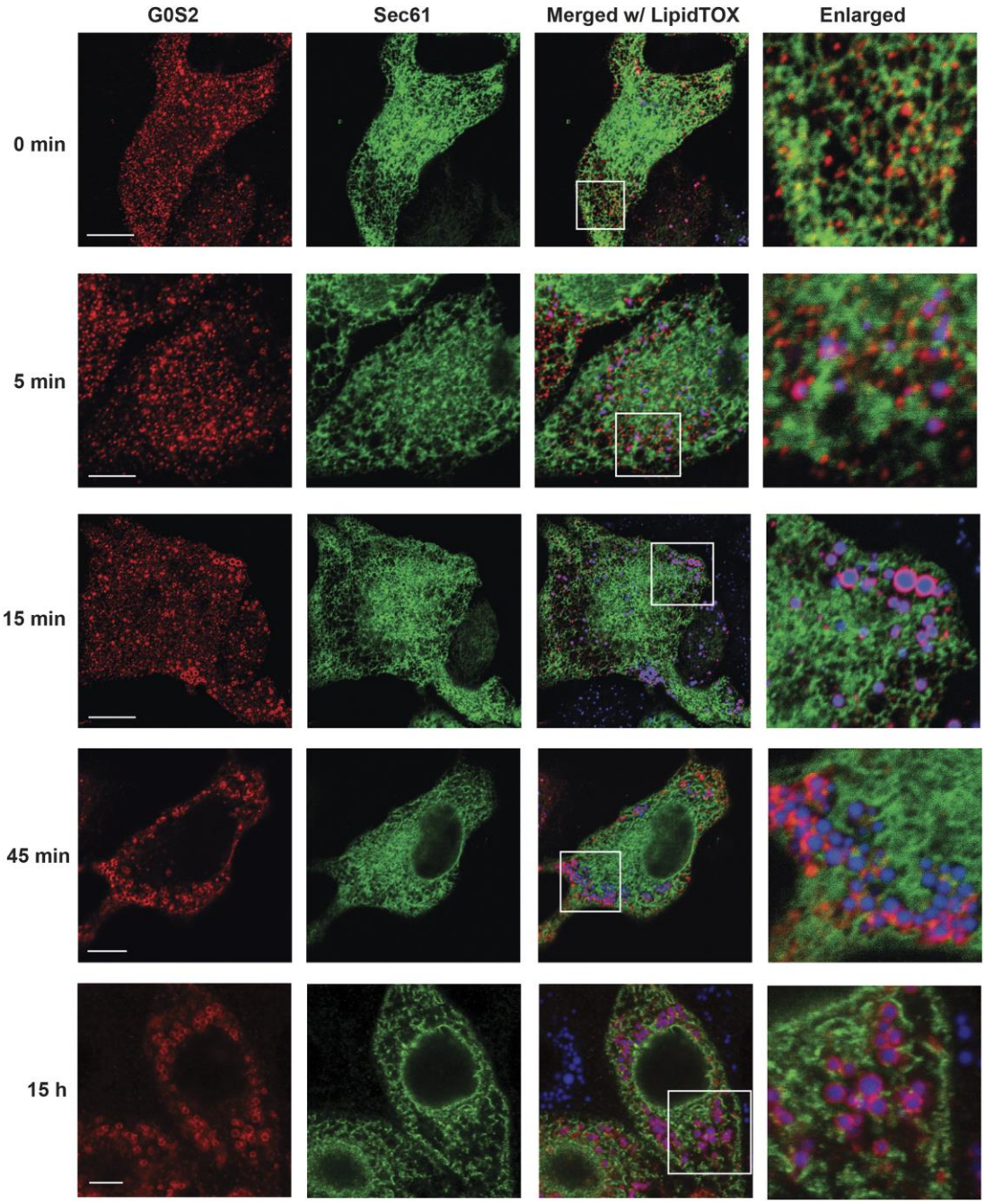

Fig. 2 Distribution of G0S2 in ER and LDs upon LD formation.

Lipid starved ATGL$^{-/-}$ HeLa cells expressing G0S2-FLAG and GFP-Sec61 were treated with oleic acid for varying lengths of time, and then imaged by immunofluorescence confocal microscopy. Scale bar: 10 μm. The white box indicates the enlarged areas.

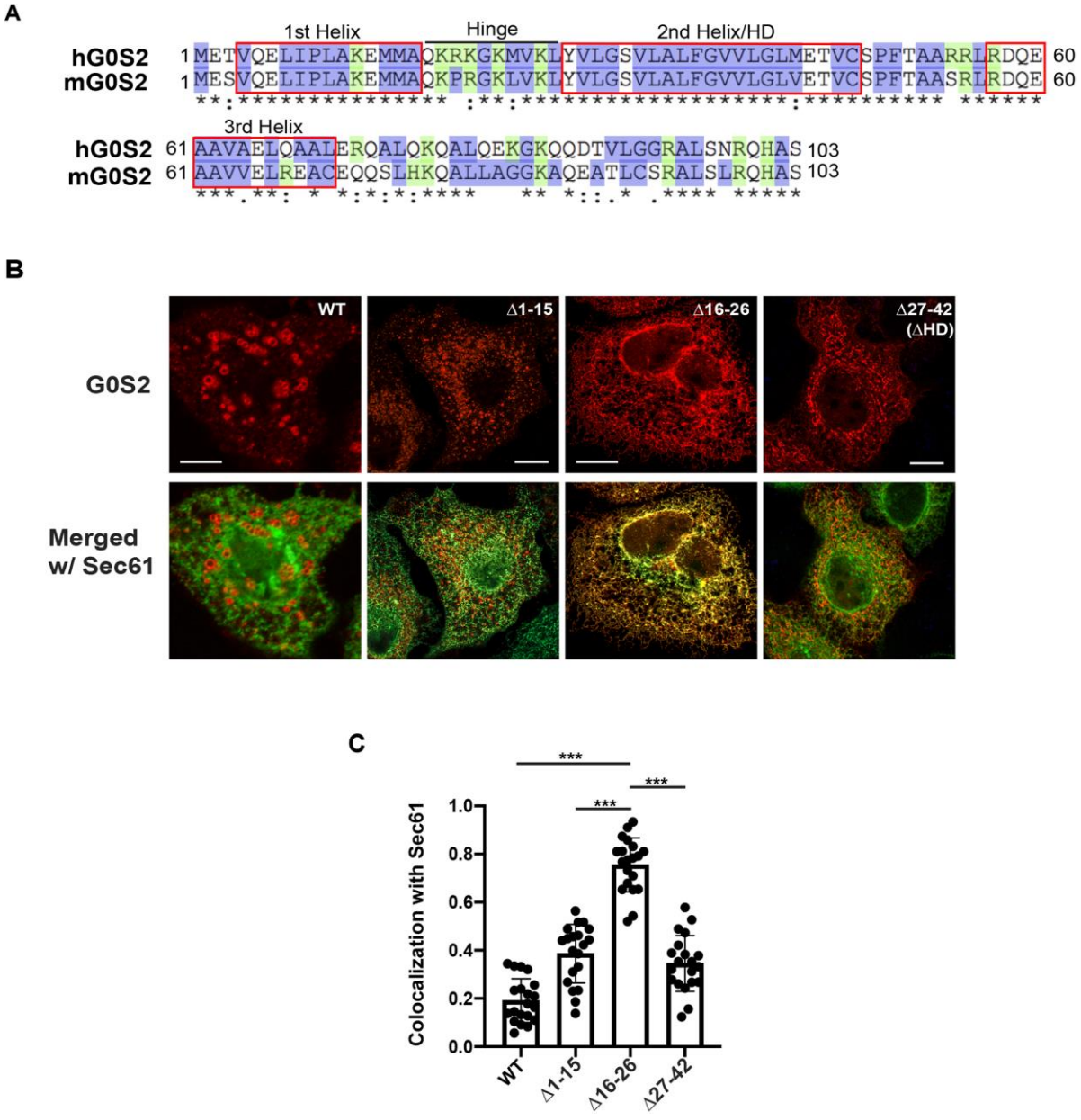

Fig. 3. The hairpin structure targets G0S2 to ER.

(A) Amino acid sequences of human and mouse G0S2 were aligned using Clustal Omega program. Overall, the sequences are well conserved with high content of basic (shown in green) and hydrophobic (shown in blue) residues. Red box contains the hydrophobic helical sequences. Identical amino acids in all proteins are marked with an asterisk (*), conservative substitutions with a colon (:), and semi conservative substitutions with a period (.). (B) HeLa cells expressing WT or deletion mutants of G0S2 along with GFG-Sec61 were treated with oleic acid and then imaged by immunofluorescence confocal microscopy. Scale bar: 10 µm. (C) Colocalization

efficiency between the G0S2 and GFP-Sec61 is shown. *, $p < 0.05$; **, $p < 0.01$. The Pearson's correlation coefficient was employed to quantitate the colocalization efficiency. Three repeats of each treatment were processed with ImageJ to obtain Pearson's correlation coefficient.

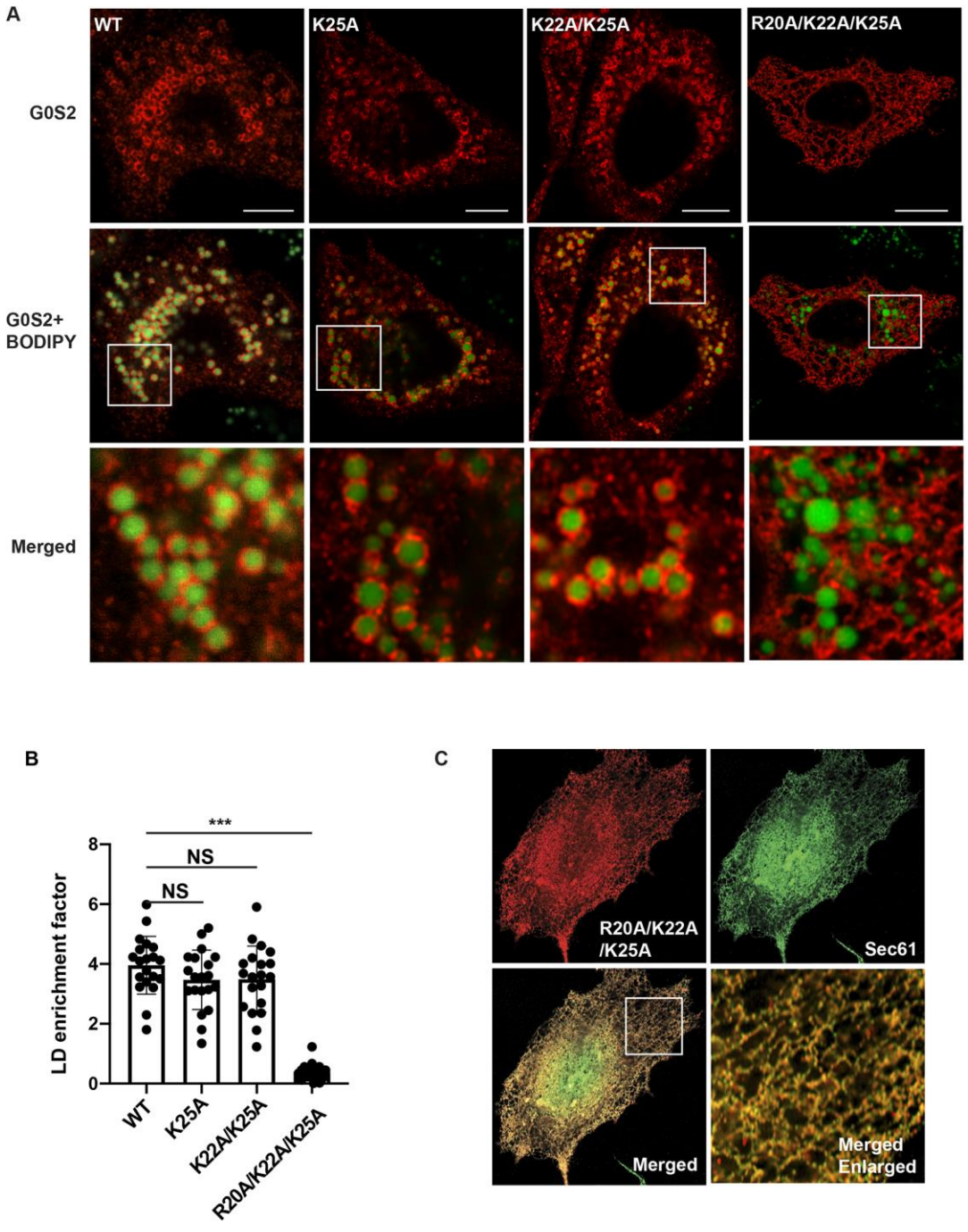

Fig. 4. Positively charged residues in the hinge region sort G0S2 from ER to LDs. (A) HeLa cells expressing WT or point mutants of G0S2 were treated with oleic acid and then imaged by immunofluorescence confocal microscopy. LDs were stained with BODIPY. (B) Mean value + SD (n = 20) of the protein signal on LDs are shown. ***$p < 0.001$; NS: no significance. (C)

HeLa cells expressing G0S2/R20A/K22A/K25A triple mutant and GFP-Sec61 were treated with oleic acid and then imaged by immunofluorescence confocal microscopy. Scale bar: 10 μm. The white box indicates the enlarged areas.

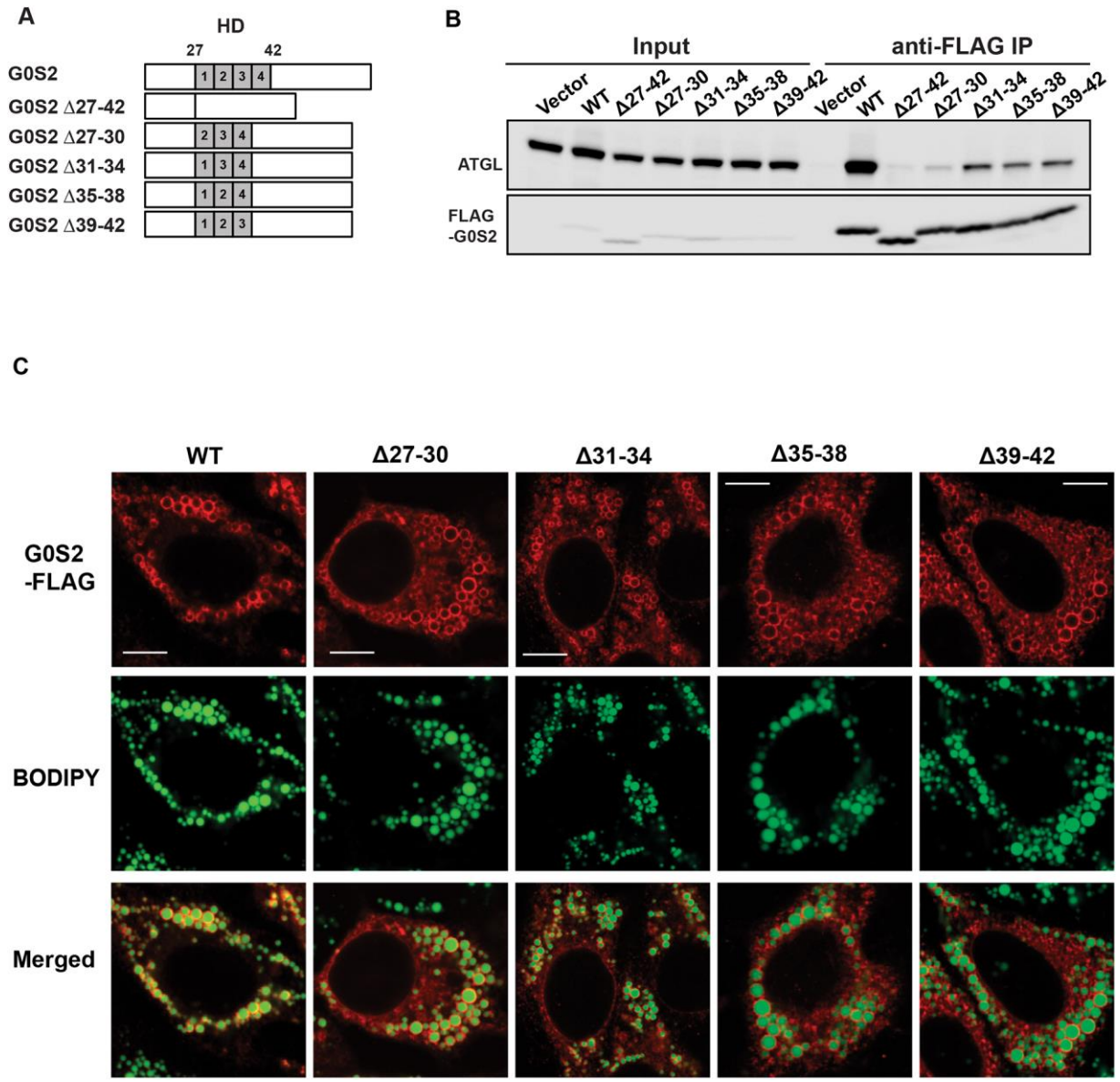

Fig. 5. The motif of G0S2 is required for ATGL interaction but for LD localization

(A) Schematic showing the structures of engineered deletion mutants of G0S2. The location of the HD domain is indicated by gray bars starting from residues 27 to 42. The HD domain was divided to 4 parts, 27–30 (1), 31–34 (2), 35–38 (3), and 39–42 (4), respectively, and the corresponding mutants were constructed with a C-terminal FLAG-tag. B) FLAG-tagged mutants were co-expressed with ATGL in HeLa cells and analyzed by anti-FLAG immunoprecipitation followed by immunoblotting. (C) HeLa cells expressing WT or deletion mutants of G0S2 were treated with oleic acid and then imaged by immunofluorescence confocal microscopy. LDs were stained with BODIPY. Scale bar: 10 μm.

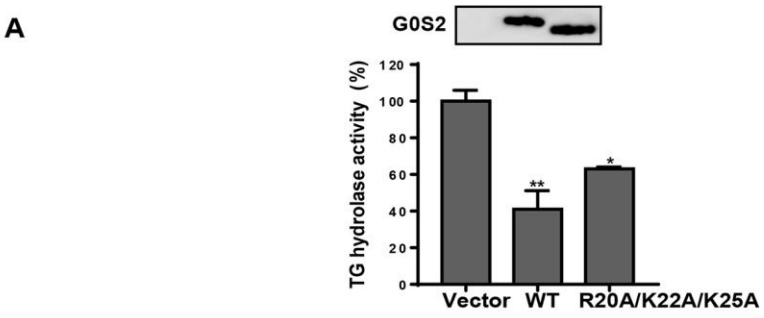

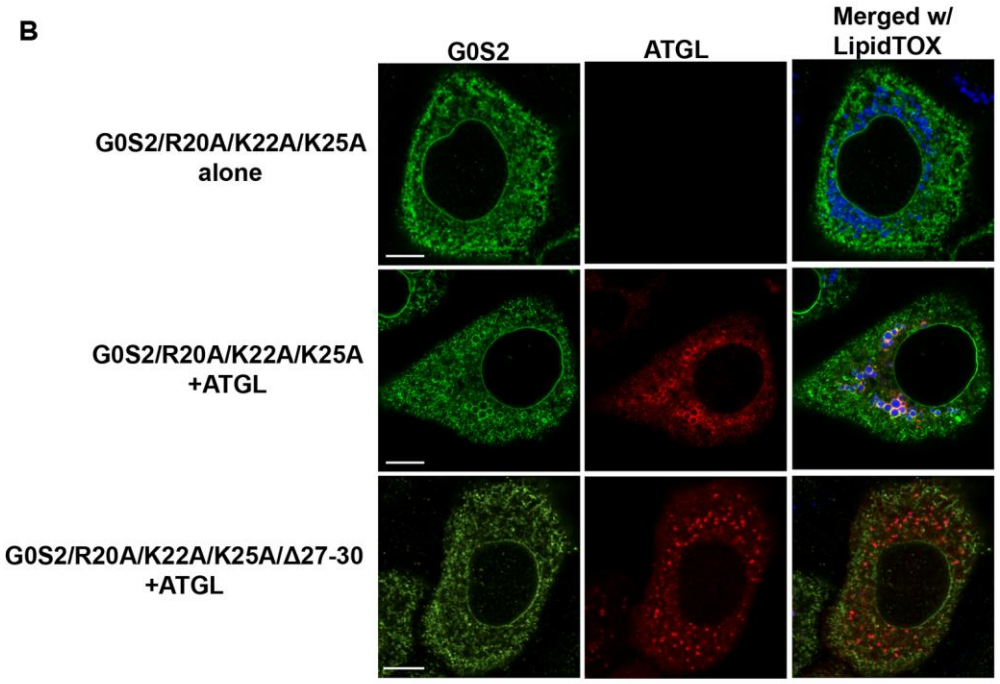

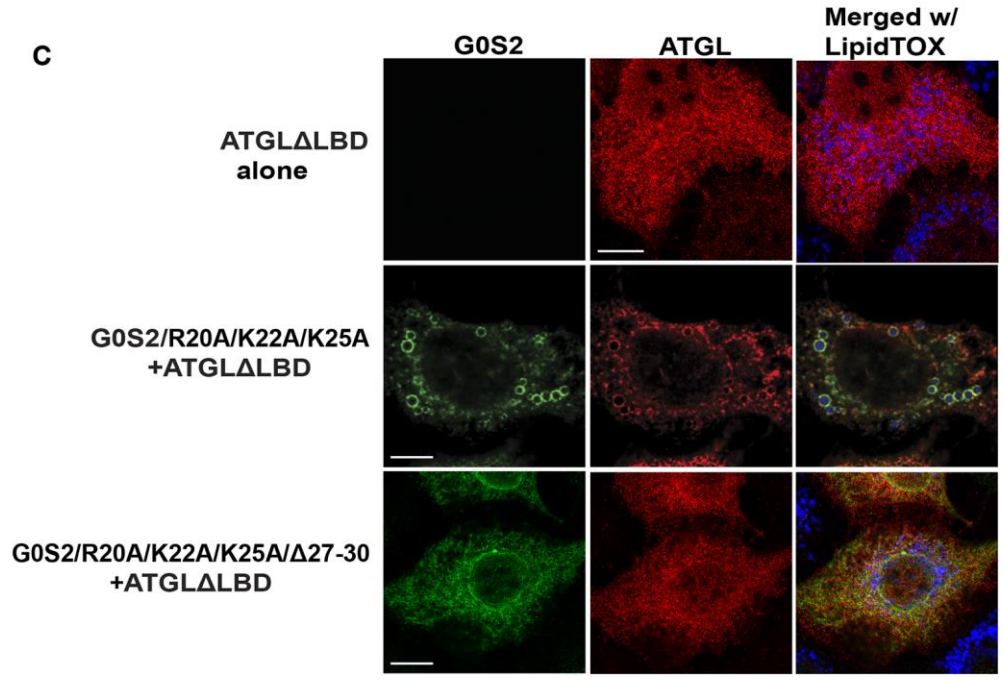

Fig. 6. ATGL coexpression promotes LD localization of G0S2 independently of positively charged residues.

(A) *In vitro* translated ATGL was mixed with WT or R20A/K22A/K25A mutant of G0S2 and TG hydrolase activity was measured using [^{3}H] triolein as substrate. The data are representative of three independent experiments. *$p < 0.05$, **$p < 0.01$ vs. vector. (B)(C) HeLa cells expressing G0S2/R20A/K22A/K25A or G0S2/R20A/K22A/K25A/Δ27-30 mutant with WT ATGL or ATGLΔLBD mutant were treated with oleic acid and then imaged by immunofluorescence confocal microscopy. LDs were stained with LipidTOX dye. Scale bar: 10 μm.

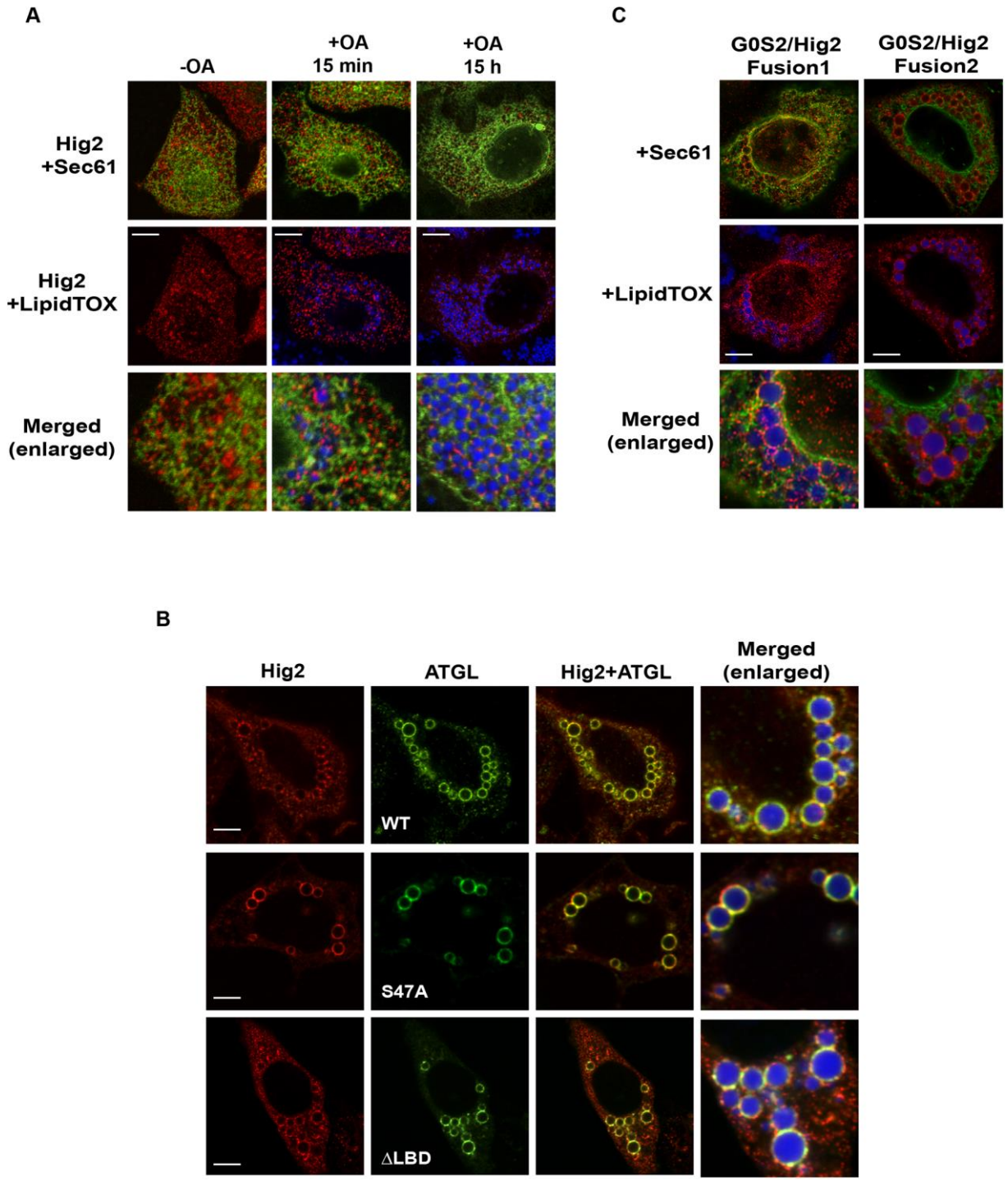

Fig. 7. Distribution of HIG2 in ER and LDs upon LD formation.

(A) Lipid starved ATGL$^{-/-}$ HeLa cells expressing HIG2-FLAG and GFP-Sec61 were treated with oleic acid for varying lengths of time. (B) ATGL$^{-/-}$ HeLa cells expressing HIG2-FLAG with WT ATGL, ATGL/S47A, or ATGLΔLBD mutant were treated with oleic acid for 15 h. (C) ATGL$^{-/-}$

HeLa cells expressing G0S2/HIG2 hybrid proteins were treated with oleic acid for 15 h. G0S2/HIG2 fusion1 contains hinge sequence of G0S2 fused to the N terminus of full length HIG2. G0S2/HIG2 fusion2 contains 1st helix and hinge sequence of G0S2 fused to the N terminus of full length HIG2. All cells were imaged by immunofluorescence confocal microscopy. LDs were stained with LipidTOX dye. Scale bar: 10 μm.

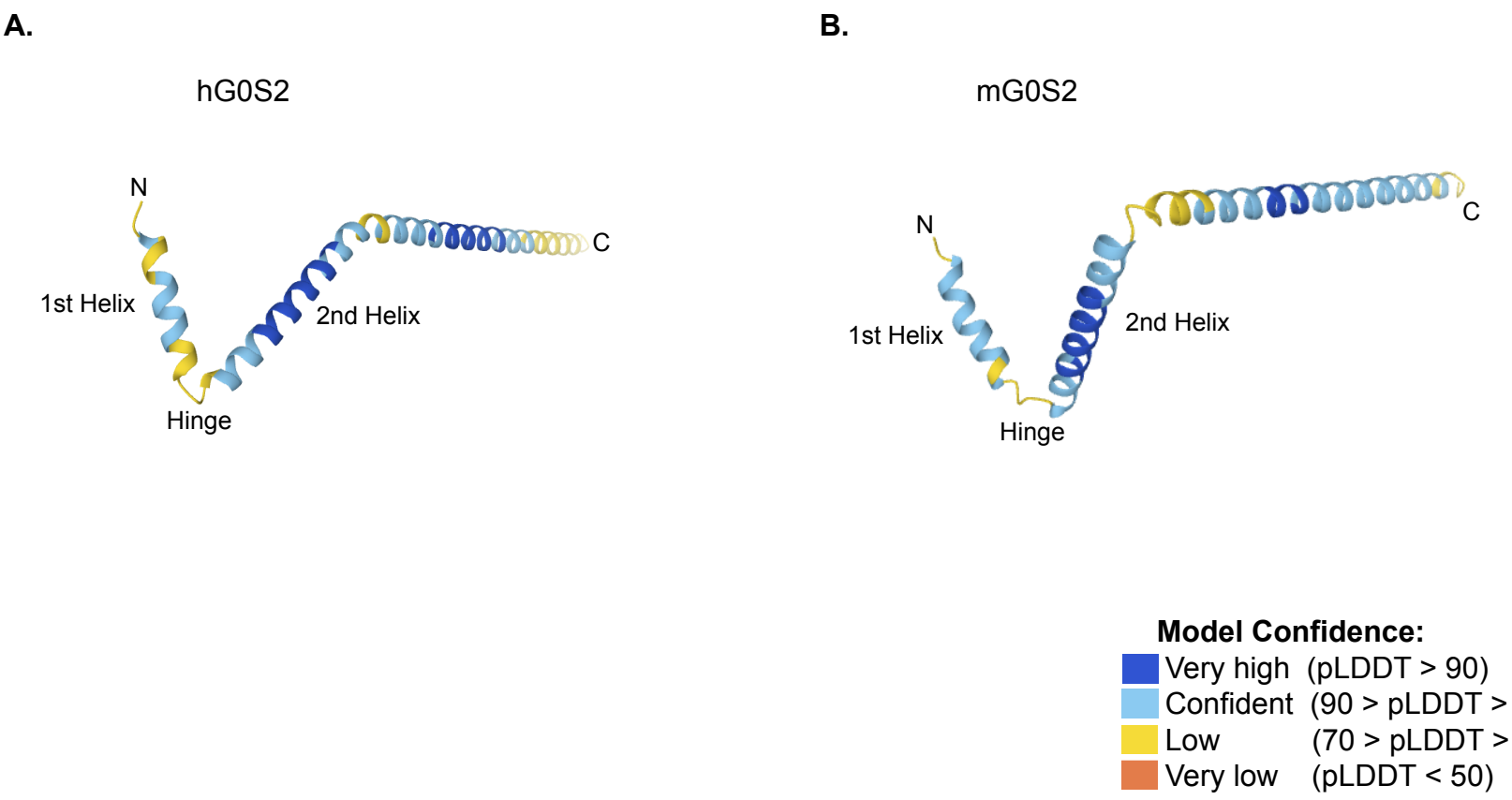

Fig. S1. Predicted structure of G0S2.

Alphafold-predicted structures of human (A) and mouse G0S2 (B) in cartoon representation. AlphaFold produces a per-residue confidence score (pLDDT) between 0 and 100. Some regions with low pLDDT may be unstructured in isolation.

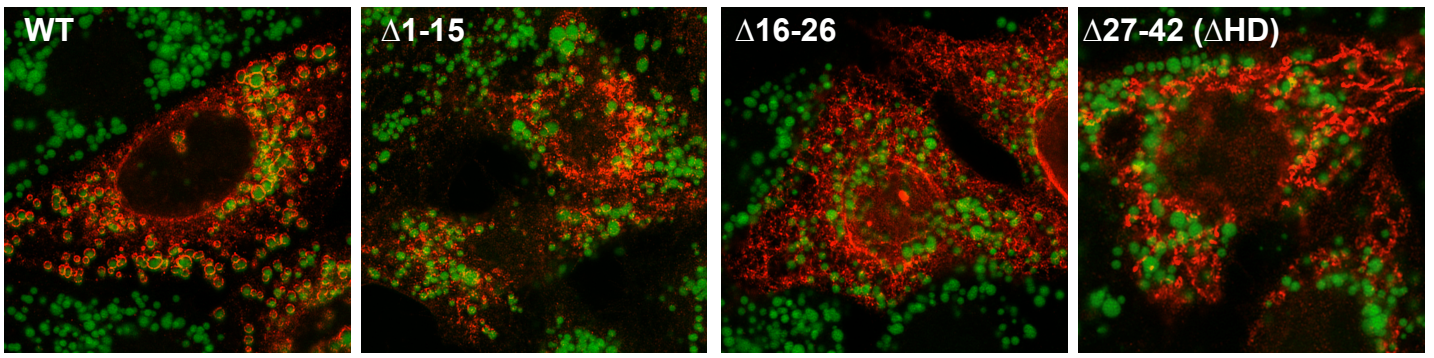

Fig. S2. Deletion of G0S2 hairpin sequences disrupts LD localization.

HeLa cells expressing WT or deletion mutants of G0S2 were treated with oleic acid and then imaged by immunofluorescence confocal microscopy. LDs were stained with BODIPY.

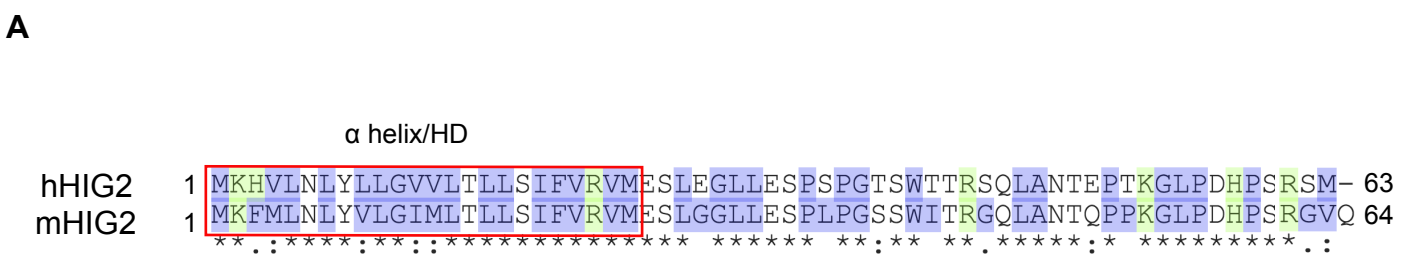

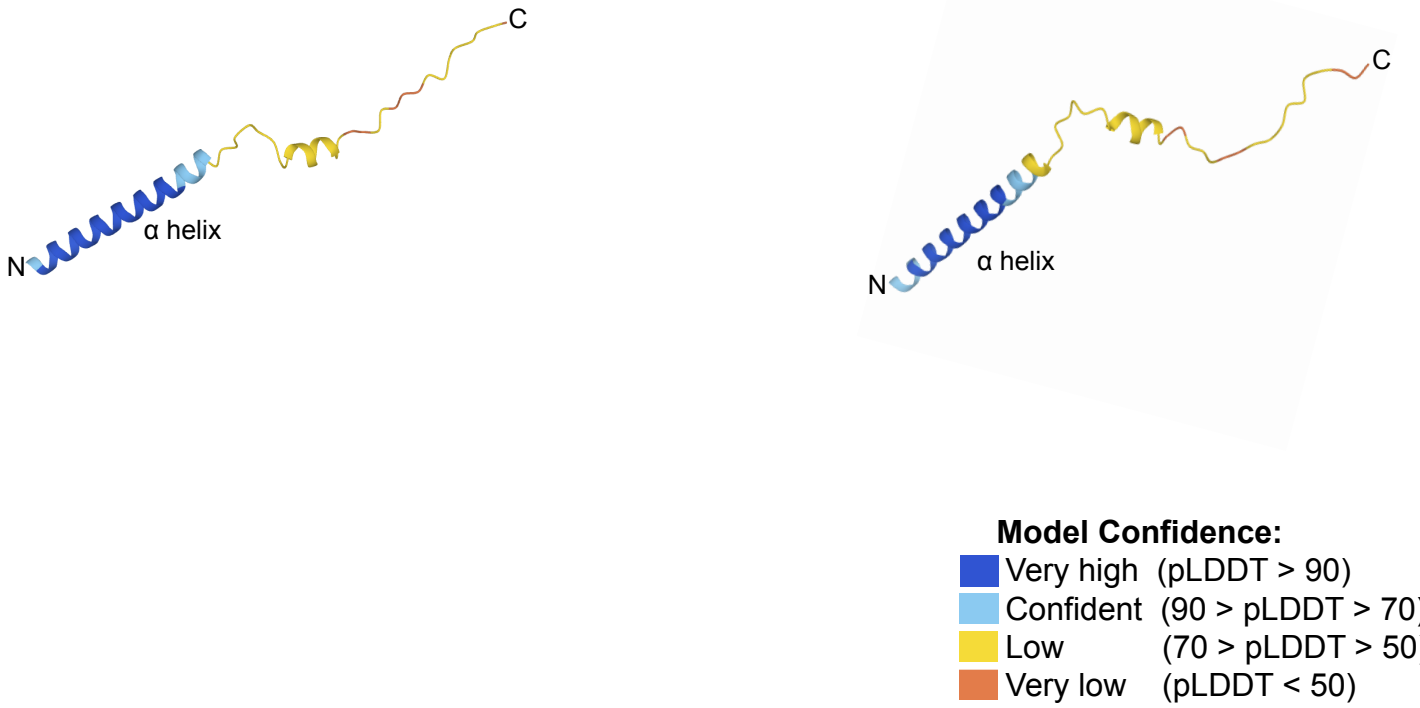

Fig. S3. Predicted structure of HIG2.

(A) Amino acid sequences of human and mouse HIG2 were aligned using Clustal Omega program. Overall, the sequences are well conserved with high content of basic (shown in green) and hydrophobic (shown in blue) residues. Red box contains the hydrophobic helical sequence. Identical amino acids in all proteins are marked with an asterisk (*), conservative substitutions with a colon (:), and semi conservative substitutions with a period (.). (B)(C) Alphafold-predicted HIG2 structure in cartoon representation. AlphaFold produces a per-residue confidence score (pLDDT) between 0 and 100. Some regions with low pLDDT may be unstructured in isolation.